A Linear AC Trap for Polar Molecules in Their Ground State†

Melanie Schnell,*,‡ Peter Lützow,‡ Jacqueline van Veldhoven,‡,§ Hendrick L. Bethlem,‡,|| Jochen Küpper,‡ Bretislav Friedrich,‡ Monika Schleier-Smith,‡ Henrik Haak,‡ and Gerard Meijer‡

Fritz-Haber-Institut der Max-Planck-Gesellschaft, Faradayweg 4-6, D-14195 Berlin, Germany, FOM-Institute for Plasmaphysics Rijnhuizen, P.O. Box 1207, NL-3430 BE Nieuwegein, The Netherlands, and Laser Centre Vrije Universiteit, de Boelelaan 1081, NL-1081 HV Amsterdam, The Netherlands

Received: February 1, 2007; In Final Form: March 23, 2007

A linear AC trap for polar molecules in high-field seeking states has been devised and implemented, and its characteristics have been investigated both experimentally and theoretically. The trap is loaded with slow $^{15}ND_3$ molecules in their ground state (para-ammonia) from a Stark decelerator. The trap's geometry offers optimal access as well as improved loading. We present measurements of the dependence of the trap's performance on the switching frequency, which exhibit a characteristic structure due to nonlinear resonance effects. The molecules are found to oscillate in the trap under the influence of the trapping forces, which were analyzed using 3D numerical simulations. On the basis of expansion measurements, molecules with a velocity and a position spread of 2.1 m/s and 0.4 mm, respectively, are still accepted by the trap. This corresponds to a temperature of 2.0 mK. From numerical simulations, we find the phase−space volume that can be confined by the trap (the acceptance) to be 50 mm^3 $(m/s)^3$.

I. Introduction

Research on cold molecules is undergoing a rapid expansion, driven by the development of a variety of methods to create cold molecules.[1] Ultracold alkali dimers in high vibrational states can be formed using photoassociation of laser-cooled atoms. By tuning a magnetic field through a Feshbach resonance, a regime of strong pairing can be reached, in which fermionic atoms bind together to form homonuclear bosonic molecules. This method has also been successfully applied to the formation of ultracold molecules in 3D optical lattices.[2] In that regime, inelastic collisions are precluded, which might enable the formation of new quantum degenerate states such as a Bose−Einstein condensate (BEC) of ground-state molecules. Buffer gas cooling combined with magnetic trapping can be applied to paramagnetic species, as has been successfully demonstrated with CaH.[3] Recently, the application of periodic optical potentials to decelerate molecules has been demonstrated with NO molecules.[4] Slow molecules can also be filtered out from an effusive beam using a bent electrostatic quadrupole guide and subsequently trapped.[5,6] Inhomogeneous electric fields can be used to decelerate and trap neutral polar molecules.[7] A successful Stark deceleration has been demonstrated for a variety of molecules such as metastable CO*,[8,9] ND_3 and NH_3,[10] OH,[11,12a] OD,[12b] YbF,[13,14] CH_2O,[15] NH,[16] SO_2,[17] and benzonitrile (C_6H_5CN); in addition, ND_3,[18] OD[12b] and OH[12a] have been trapped. The above techniques have made it possible to exert an unprecedented control over the motion of neutral molecules. Once at a quasi-standstill in the laboratory frame, the molecules can be confined in a trap.

The use of cold molecules offers unique possibilities for novel molecular beam experiments, such as studying cold collisions[19−24] or dipole−dipole interactions,[25−27] or for high-resolution spectroscopy[28,29] due to longer observation times. In each of these applications, traps are either necessary, or they considerably enhance the potential of the method in question. Different trapping schemes for molecules using static electric or magnetic, AC electric, and optical fields have been developed during recent years.

Generally, one has to differentiate between molecules in states whose Stark (Zeeman) energy increases when the molecules enter an increasing electric (magnetic) field; these are the so-called low-field seekers (lfs). Molecules in states whose Stark (Zeeman) energy decreases when they enter an electric (magnetic) field are correspondingly called high-field seekers (hfs). Molecules in lfs states can be trapped in static electric or magnetic fields. Such traps are highly versatile. They are rather deep (on the order of 1 K), and by changing the electrode geometries or the applied voltages, a variety of trapping potentials can be created.[12a,18,30−34]

The ability to trap molecules in their hfs states is of special importance because all molecular ground states as well as the majority of states of larger molecules are hfs. This is important for techniques that provide further cooling such as evaporative cooling, a key step in reaching quantum degeneracy. For evaporative cooling, the trapped molecules have to undergo elastic collisions in order to thermalize. Trapped molecules in lfs states can also partake in inelastic collisions that may result in an untrapped hfs state; consequently, the lfs are lost from the trap. Because the hfs ground-state molecules cannot decay, they can be subject to an efficient evaporative cooling.

In order to confine molecules in hfs states, time-dependent trapping fields have to be relied upon. Although Maxwell's equations forbid a maximum of a static magnetic or electric field in free space, it is possible to create an electric field such

† Part of the "Roger E. Miller Memorial Issue".

* To whom correspondence should be addressed. Tel: +49-3084135604. Fax: +49-3084135604. E-mail: schnell@fhi-berlin.mpg.de

‡ Fritz-Haber-Institut der Max-Planck-Gesellschaft.

§ FOM-Institute for Plasmaphysics Rijnhuizen.

|| Laser Centre Vrije Universiteit.

10.1021/jp070902n CCC: $37.00
Published on Web 06/13/2007

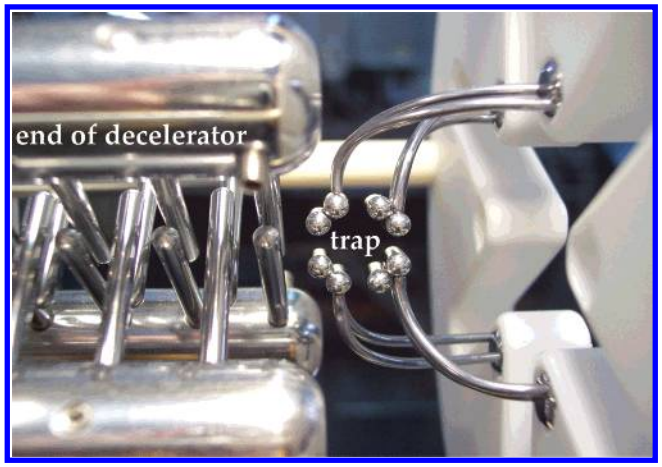

Figure 1. Picture of the very open linear AC trap combined with the Stark decelerator. The trap is held by bent tantalum wires that are suspended from a ceramic plate.

that a saddle point is generated in the trap center. By switching between two complementary saddle point configurations, stable trapping can be obtained. Three different geometries for AC traps are possible:[35] a linear trap, a cylindrically symmetric trap, and a so-called 3-phase trap. Recently, van Veldhoven et al.[35,36] implemented the first AC electric trap for ground-state molecules, consisting of a pair of cylindrically symmetric ring electrodes and a pair of endcap electrodes.

Other approaches to trapping molecules in hfs states rely on optical or microwave fields. Molecules in hfs states have been trapped in the focus of a CO_2 laser beam. The light traps thus far demonstrated have typically a trap depth of a few hundred μK and a volume of 10^{-5} cm^3.[37] A microwave trap, in which polar molecules in hfs states are supposed to be trapped in the standing-wave maximum of a microwave field, has been proposed with possible trap depths of up to 100 mK for a molecule with a 1 D dipole moment.[38]

In the present work, we demonstrate, for the first time, a linear AC trap, which is located immediately behind a Stark decelerator. Its open geometry offers optimal access. In addition, with this linear geometry, it is possible to load hfs molecules directly into the trap. The linear trap could be equally well combined with an alternate gradient (AG) decelerator[9,14] for molecules in hfs states. This would widen the scope of the species amenable to deceleration and efficient trapping to large molecules, which possess only hfs states. The ability to cool and trap large molecules would be of importance to spectroscopy and metrology. In the following we report the experimental and theoretical characterization of the linear trap.

Our article is organized as follows: in section II, we describe the trapping principle and the trap itself, and in section III, we describe the experimental procedure. In section IV, we introduce our numerical simulations, whereas in section V the experimental and theoretical results of our investigation are discussed. Section VI provides the summary and conclusions.

II. The Trap

The trap consists of four 8 mm long double-rod electrodes of 3 mm diameter each, fashioned from highly polished stainless steel. The individual electrodes are set up in a quadrupole arrangement (Figure 1), held in place by bent tantalum wires ($\phi = 1.5$ mm) that are suspended from a ceramic plate. Tantalum was found to be a good material to prevent the occurrence of discharges in experiments using high voltages. The combination of this novel and compact manner of holding the trap together

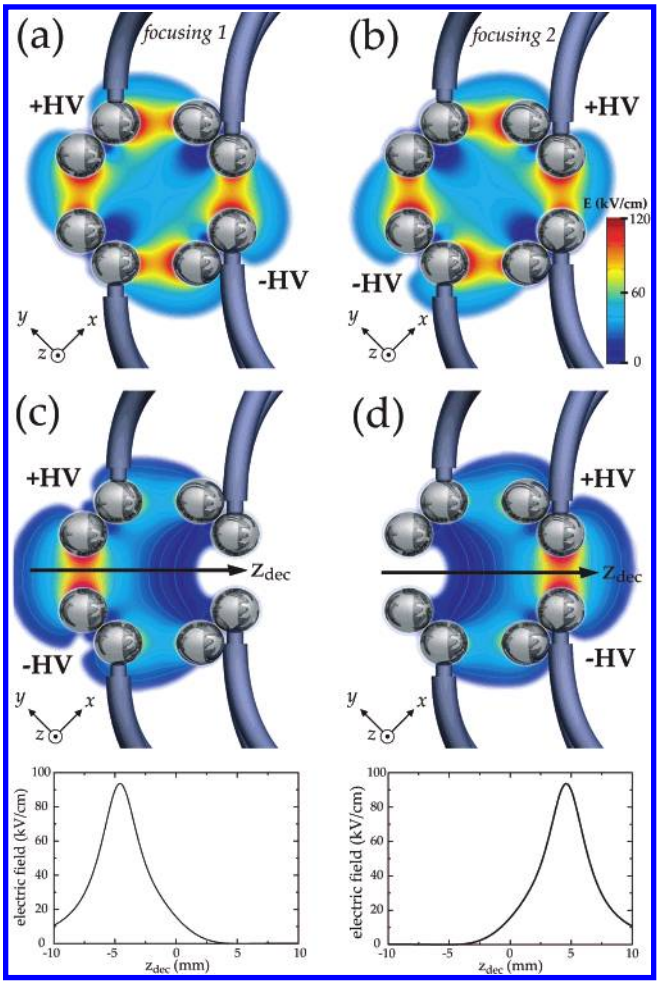

Figure 2. Four different electric field configurations of the AC trap used in the course of an experiment. Parts a and b show the two different saddle point configurations (*focusing 1* and *focusing 2*) of the linear AC trap. Trapping in the third dimension along the *z*-axis is due to fringe field effects of the electric field strength. (c) Electric field strength corresponding to the deceleration stage of the trap. The left electrode pair is energized with high voltages of up to $\pm$10 kV, while the right pair is grounded. The electric field strength along the molecular beam axis z_{dec} is given below. The trap center is at $z_{dec} = 0$ mm. This configuration can also be used to load molecules in hfs states into the trap. (d) Loading configuration. The left electrode pair is grounded, while the right one is energized (up to $\pm$10 kV). The electric field strength along the molecular beam axis z_{dec} is displayed below. The color scale indicator in part b also applies to the electric field configurations shown in a and c−d.

along with the trap's geometry makes it possible to place the trap very close to the end of the decelerator. With this arrangement, the trap can be directly loaded from the decelerator without a need for any additional focusing devices.

As discussed in ref 35, the demonstrated cylindrically symmetric AC trap has a larger trap depth for molecules in lfs states compared to that in hfs states. Initially, we thought that electrodes with a concave shape, which can be mimicked with the double-rod geometry displayed in Figure 1, might reverse this situation, i.e., form a deeper trap for hfs than for lfs. In the course of our studies, this turned out not to be the case. A single-rod arrangement[35] would in fact improve the trap depth compared to the double-rod trap. Nevertheless, the present geometry allows for an open geometry and thus for optimal access.

Parts a and b of Figure 2 show the simulated electric field strength distributions for the two different trapping configura-

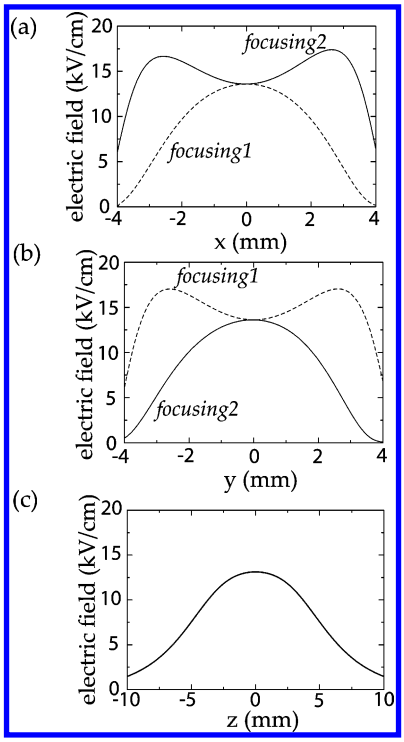

Figure 3. Electric field for the two focusing configurations in *x*-, *y*-, and *z*-directions. The electric field in the *z*-direction is the same for the two configurations.

tions of the linear AC trap (calculated using the finite element program package COMSOL Multiphysics). In the switching configuration displayed in part a, the electrodes on the *y*-axis are energized, while the other two are grounded. An electric field is generated in which molecules in hfs states are focused in the *x*-direction, while being simultaneously defocused in the *y*-direction (*focusing 1*). For *focusing 2* (part b), the electrodes on the *x*-axis are on high voltage, and the resulting electric field is just reversed (simultaneous defocusing in the *x*-direction and focusing in the *y*-direction). Typically, high voltages up to ± 10 kV have been applied to energize the electrodes.

Figure 3 shows the dependence of the electric field strength on the *x*-, *y*-, and *z*-coordinates for the two focusing configurations and displays the two complementary saddle point configurations. Whereas in the *x*-direction there is a maximum of the electric field for *focusing 1*, a minimum is generated in the *y*-direction and vice versa (*focusing 2*). Focusing in the third dimension (*z*-axis) is due to fringe field effects. Along the *z*-axis, the electric field has a maximum at $z = 0$ (Figure 3c); therefore, molecules in hfs states experience a (static) trapping potential along this direction. In contrast to the cylindrically symmetric AC trap,[36] molecules in lfs states cannot be trapped but are pushed out from the linear trap.

Because of the static confinement along the *z*-direction, the defocusing forces in the *x*- and *y*-directions are always somewhat stronger than the focusing forces. Nevertheless, stable trapping can be obtained. Generally, the magnitude of the force on a molecule is proportional to the distance from the center of the trap. Because a molecule does not stay at a fixed position but moves toward the center of the trap under the influence of a focusing force, it will then be closer to the center where the force is smaller at the time when the defocusing force is applied. This defocusing force moves the molecule further away from the center again, bringing it to the region of a larger force when the focusing force is applied. On average, molecules are further away from the center of the trap when the focusing force is

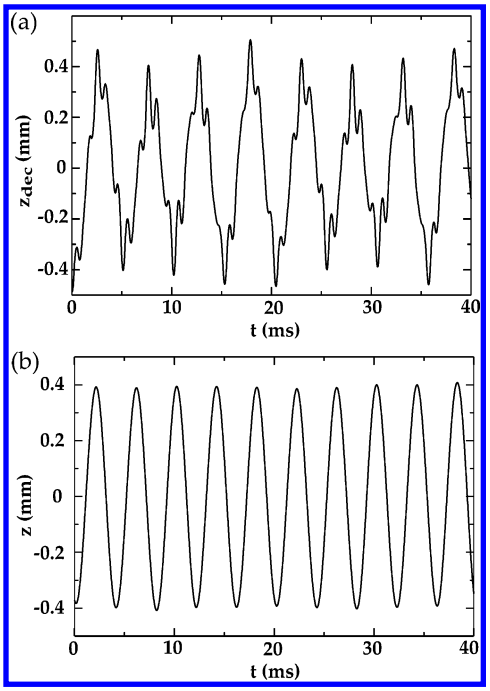

Figure 4. Trajectory of an ammonia molecule ($^{15}ND_3$) along the molecular beam axis z_{dec} (a) and along the *z*-axis of the trap (b) as a function of time. The switching frequency is 1150 Hz.

applied than they are while being defocused, resulting in a net focusing force. If the molecules are in a stable trapping region, they perform a slow "secular" oscillation around the center of the trap under the influence of this force on which a fast "micro" motion at the switching frequency is superimposed. This can be seen in Figure 4a, where the trajectory of an hfs ammonia molecule in the linear AC trap along the molecular beam axis z_{dec} is displayed. In addition, the molecules perform an oscillation in the static electric field along the *z*-axis (Figure 4b).

Parts c and d of Figure 2 show the loading scheme of the trap: the molecules approach the trap from the left along the molecular beam axis z_{dec}. The first electrode pair of the trap can be used as the last decelerator stage so that, in the ideal case, the molecules will not notice the transition from the decelerator to the trap. Because the trap offers this additional deceleration stage, the molecules can leave the decelerator with a higher velocity so that a smaller phase angle can be used for the deceleration process,[7] and thus more molecules can be decelerated. The molecules are also focused by the deceleration fields of the trap when flying from the decelerator to the trap center. As the next step, the molecules are loaded into the trap, i.e., brought to a quasi stand-still in the trap center. Consequently, one trapping experiment comprises four different electric field configurations of the linear AC trap for deceleration (Figure 2c), loading (Figure 2d), and trapping (Figures 2a and b). The field configuration shown in Figure 2c can also be used to load molecules in hfs states into the trap. They will be brought to a quasi-standstill by letting them fly out of the electric field.

III. Experimental Section

The experimental setup is shown in Figure 5. In the experiments described here, the trap is loaded from a Stark-decelerated molecular beam. A more extensive description of this part of the setup, along with the operation principle of the decelerator, can be found elsewhere.[10,28] A mixture of 5% $^{15}ND_3$ seeded in xenon is supersonically expanded from a pulsed valve at a 10 Hz repetition rate. The rare isotopologue $^{15}ND_3$ is

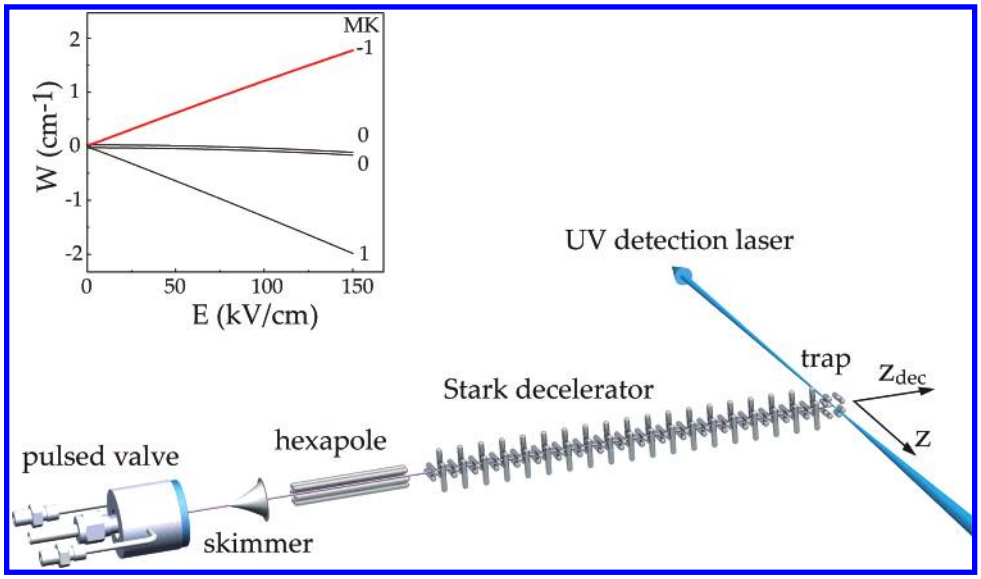

Figure 5. Experimental setup and Stark effect behavior of ND_3. Note the two different coordinate systems which are used to describe the experiment.

mainly used for two reasons. First, compared to NH_3, ND_3 has a significantly smaller inversion splitting resulting in a more linear Stark effect. Consequently, ND_3 can be Stark decelerated more effectively. Second, $^{15}ND_3$ exhibits no quadrupole hyperfine structure like $^{14}ND_3$ does, but only spin-rotation coupling ($I(^{14}N) = 1$, $I(^{15}N) = 1/2$), which results in a much narrower splitting.[39] Thus, a higher fraction of molecules can be pumped from the lfs to the hfs state using one resonant microwave pulse, as described below. Because of the cooling of the valve to −70 °C , the molecules in the beam have a most probable velocity of 280 m/s. In the expansion, about 60% of the ammonia molecules are internally cooled to the ground state of para-ammonia, the $|J, K\rangle = |1, 1\rangle$ inversion doublet in the electronic and vibrational ground state. After passing through a skimmer, which is located 35 mm downstream from the nozzle, those molecules that reside in the lfs hyperfine levels ($MK = -1$, the upper component of the inversion doublet; Figure 5) are focused into the Stark decelerator by a 6 cm long hexapole. Molecules in hfs levels ($MK = +1$, Figure 5, the lower component of the inversion doublet) are attracted by the high electric fields of both the hexapoles and the decelerator and are lost from the beam. Molecules which reside in the remainder of the hyperfine levels of the inversion doublet ($MK = 0$, Figure 5) only have a higher-order Stark effect and are hardly affected by the electric fields.

The decelerator consists of 95 pairs of two parallel 3 mm diameter rods, with a closest distance of 2 mm between two rods and a closest distance of 2.5 mm between adjacent pairs of rods. Each consecutive pair of rods is rotated by 90° to guarantee transverse focusing. Within each pair, a positive voltage of 10 kV is applied to one electrode and the same negative voltage to the other electrode. Using phase angles of 57.5° and 57.2°, a subset of molecules in lfs states is decelerated to about 15 and 25 m/s, respectively, at the end of the decelerator.

When the molecules exit the decelerator, they are subject to yet another deceleration process while approaching the trap (Figure 2c), followed by the loading according to Figure 2d. By gaining Stark energy when entering the trap, the molecules in lfs states lose their remaining kinetic energy and reach a standstill at the trap center. At that moment, a resonant microwave pulse of 20 μs duration is coupled in using a dipole antenna to induce a transition from the lfs to the hfs hyperfine levels in the $|J, K\rangle = |1, 1\rangle$ state of $^{15}ND_3$.[28] Under typical conditions, about 20% of the ammonia molecules are pumped to hfs levels. This pumping efficiency is limited because of the width of the applied microwave pulse and the spin-rotation hyperfine structure. The frequency of the zero-field transition is 1.43 GHz for $^{15}ND_3$.

After the formation of slow hfs $^{15}ND_3$ molecules in the center of the trap, the AC electric trap is turned on. After holding the molecules for a certain time, the trap is turned off, and molecules in the lower component of the inversion doublet (hfs state) are ionized in a state-selective (2 + 1)-resonance enhanced multi photon ionization (REMPI) scheme, using a pulsed UV-laser around 321 nm.[40] For the investigation of the loading procedure, molecules in the upper component (lfs states) can also be state-selectively ionized using (2 + 1)-REMPI (around 317 nm[40]). The resulting ions are detected in a time-of-flight (TOF) mass-spectrometer. Using a 75 cm lens, the ionization laser is focused into the trap. Because of the open trap geometry, optimal optical access for the ionization laser is guaranteed. The laser focus is estimated to be about 200 μm in diameter. Applying small bias voltages of 200 V to both electrodes of the first electrode pair and −100 V and −125 V to the electrodes of the second pair results in an electric bias field that accelerates the ions toward the detector. The acceleration voltages have to be applied in a slightly asymmetric arrangement in order to correct for small misalignments of the trap. The ions can be detected over a length of about 4 mm along the laser beam. Using a computer-controlled translation stage, the laser focus can be moved along the molecular beam axis over the whole transversal width of the trap, enabling the experimental characterization of the spatial distribution of the trapped molecules.

IV. Numerical Simulations

We performed numerical calculations to simulate our experiments and to provide a better understanding of the trap characteristics. In the first step, the four different electric field configurations displayed in Figure 2 as well as the electric field configurations of the Stark decelerator have been simulated using a finite element program (COMSOL Multiphysics). The magnitude of the electric field and the field gradient vectors were exported on a grid with sampling periods of 0.1 mm and were integrated in the program package libcoldmol[41] which allows one to numerically calculate, using the Monte Carlo method, the trajectories of the molecules in a molecular packet through the molecular beamline as a function of time.

The force fields $m\cdot\vec{a}$ for the molecules as a function of their position $\vec{r}$ have been calculated using the simulated electric fields and gradients, obtained directly from COMSOL Multiphysics, and the Stark energy W and mass m of the molecules according to

$$m\cdot\vec{a}(\vec{r}) = \mu_{\text{eff}}(E(\vec{r}))\cdot\nabla\vec{E}(\vec{r}) \quad (1)$$

with the effective dipole moment μ_{eff} of the molecule for a given electric field strength $E = |\vec{E}|$

$$\mu_{\text{eff}}(E(\vec{r})) = -\left(\frac{\partial W}{\partial E}\right)_{E(\vec{r})} \quad (2)$$

The Stark energy of the $^{15}ND_3$ molecules in their $|J\,K\rangle = |1\,1\rangle$ state was calculated according to[42]

$$W(E) = \pm\sqrt{\left(\frac{W_{\text{inv}}}{2}\right)^2 + \left(\frac{\mu E}{2}\right)^2} \mp \frac{W_{\text{inv}}}{2} \quad (3)$$

with $W_{\text{inv}} = 1430.336$ MHz[28] and $\mu = 1.48$ D.[43]

We created initial molecular packets using Gaussian (z, v_x, v_y, v_z) or uniform (x, y) random distributions in phase space. By integrating the equation of motion using the Runge−Kutta formalism (Cash−Karp (4,5) or Prince−Dormand (8,9)) the trajectories of typically one million molecules were calculated. We were able to simulate the whole experiment, starting from the nozzle, including the deceleration process in the Stark decelerator and the trap, the loading, and the trapping. The results of these simulations fit the experimental results well and are presented along with the experimental data in the following section.

V. Results and Discussion

A. Deceleration and Loading. Figure 6 shows time-of-flight measurements of ammonia molecules in lfs states for different experimental conditions relative to the time when the valve opens ($t = 0$ ms). The detection laser beam is located in the trap center, 12 mm downstream from the end of the decelerator. Curve 6a shows the characteristic Gaussian type arrival time distribution of the original molecular beam when the decelerator is off, i.e., after 0.675 m of free flight. The maximum of the distribution is found around 2.7 ms after opening the valve. Curve 6b displays the time-of-flight profile when the molecules are decelerated from 280 to 25 m/s (phase angle 57.2°) and all voltages of the trap are switched off. At the entrance of the decelerator, the beam has an extension along the molecular beam axis of about 25 mm (FWHM). This is more than twice as long as the spatial period of the decelerator, and thus, more than one bucket will be filled. Two peaks are clearly observed in the TOF profile (around 4.2 and 4.75 ms, curve b). The later peak originates from molecules that were at the right position near the entrance of the decelerator at the start of the deceleration time sequence and that passed through all 96 deceleration stages. At the exit of the decelerator, this decelerated packet contains about 10^6 molecules and has a $2 \times 2 \times 2$ mm^3 volume. The corresponding molecules entered the decelerator with a velocity of 280 m/s and exited with 25 m/s. The earlier peak originates from molecules that were already one period further inside the decelerator at the start of the deceleration time sequence. These molecules also entered the decelerator with a velocity of 280 m/s, but because they missed the last two deceleration stages, they left the decelerator with a slightly higher velocity. For further details see, for example, ref 44. Because of the transverse focusing of the beam, the signal intensity typically increases

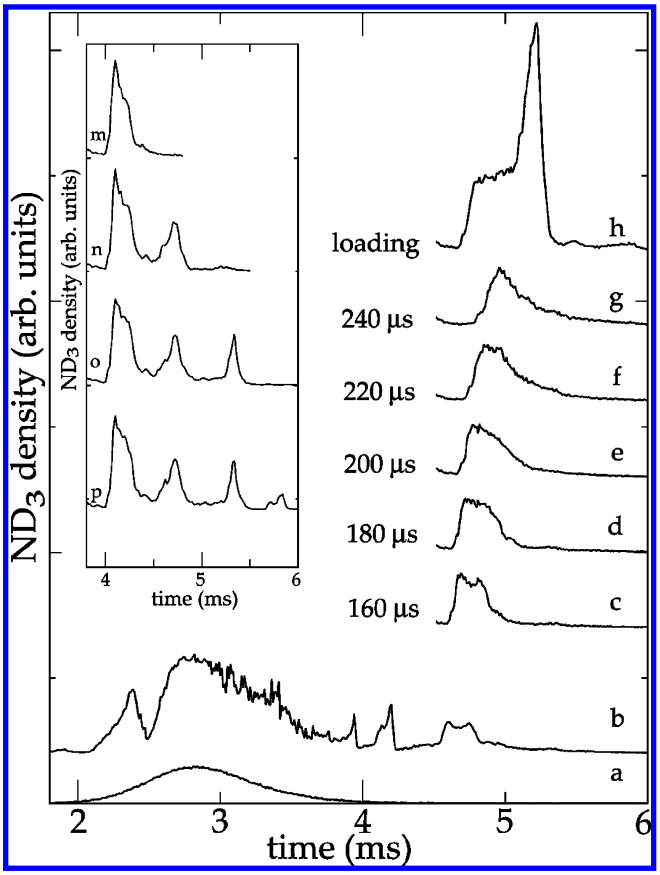

Figure 6. Time-of-flight (TOF) spectra characterizing the deceleration and loading process. The detection laser is located in the trap center and is tuned to a REMPI-frequency resonant for molecules in lfs states. Curve a shows the Gaussian type distribution of the original beam when no fields are turned on. Curve b was obtained with only the decelerator turned on, resulting in a packet of molecules slowed down to 25 m/s (TOF of 4.7 ms). For curves c−g, the deceleration stage of the trap has been turned on for different time intervals, as indicated in the Figure. Curve h displays the strong focusing effect that is obtained when, in addition to the trap deceleration field (on for 200 μs), the loading field is also turned on for 690 μs. The voltage applied to the decelerator and trap electrodes is ±10 kV. The inset shows the TOF spectra for reflection experiments with $^{15}ND_3$ molecules in lfs states using the deceleration and loading fields of the trap (see text). For all curves, the measured signal is zero for larger times approaching 6 ms.

when the decelerator is switched on. This can also be seen for the remaining part of the original beam (around 2.7 ms) in curve b.

The advantages of the novel mounting configuration, which allows the trap to be located directly behind the decelerator, become immediately apparent when examining the signal intensities obtained in the present measurements. As can be seen from Figure 6, the signal intensity of the molecules decelerated to 25 m/s (at 4.75 ms, curve b) is about the same as that for the signal of the original beam (curve a). It should furthermore be noted that all hyperfine structure levels of the upper inversion component, i.e., with $MK = 0, -1$, contribute to the signal of the original beam, whereas only a fraction, i.e., with $MK = -1$, contributes to the guided signal when the decelerator is switched on.

In curves 6c−g (Figure 6), the deceleration field of the trap is turned on, in addition, over varying time intervals. When the deceleration field of the trap is also turned on, the decelerated molecules are slowed down further and focused stronger, as the free flight of the molecules inside the trap is curbed. The focusing effect has two different contributions: transverse

(resulting in a higher peak intensity) and longitudinal (resulting in a narrower peak). Between the two entrance electrodes of the trap, the field strength is increasing in one transverse direction (Figure 2). Consequently, molecules with a nonzero velocity component are focused back toward the molecular beam axis. In the *z*-direction, however, the molecules are not focused. In the longitudinal direction, molecules that have a larger longitudinal velocity v_{dec} than that of the synchronous molecule (for the concept of the synchronous molecule see, for example, ref 7) are decelerated more than molecules that lag behind the synchronous molecule. The velocity spread of the molecules in the packet is thus reduced, resulting in the measured longitudinal focusing effect (bunching). With longer times, the packet eventually becomes broader again. A good compromise between deceleration and focusing is obtained when the deceleration stage of the trap is turned on for 180−220 μs (curves d−f in Figure 6).

Curve h of Figure 6 shows time-of-flight measurements when the loading configuration is also turned on. The decelerator stage was on for 200 μs. The optimal loading time was experimentally found to be 690 μs for ±10 kV. As a result of the loading, the synchronous molecule of the decelerated packet is brought to a standstill in the trap center. In the deceleration process, its reduced position (spatial phase) is always the same at the time the fields are switched, and the kinetic energy of the molecule changes by a constant amount per stage (see, for example, refs 7 and 45). Note that the peak intensity for the loaded molecules is about 8 times stronger than that for the decelerated packet in curve b. As mentioned above, this remarkably strong signal is due to the integration of the trap with the decelerator and the improved loading scheme.

The deceleration and loading fields of the trap can also be used to reflect polar molecules, as shown in the inset in Figure 6. The reflection of polar molecules has first been demonstrated with decelerated ND_3 molecules using a microstructured mirror.[46] A similar macroscopic setup has recently been used to reflect hydrogen atoms in an excited Rydberg state.[47] For our measurements, the detection laser focus is placed in the trap center, i.e., 12 mm downstream from the decelerator. Curve m (Figure 6, inset) shows the molecular packet, which has been decelerated to 35 m/s using the Stark decelerator, and the deceleration stage of the trap. It arrives in the trap center about 4.2 ms after the gas pulse. In curve n (Figure 6, inset), the loading configuration has been turned on immediately after the deceleration stage. In this experiment, however, the molecules are too fast so that they cannot be brought to a standstill in the trap center using the potential hill of the loading configuration. Instead, their longitudinal velocity is reversed about 3 mm downstream from the trap center. A significant fraction of the molecules will thus be reflected, while some molecules, namely, the fastest ones, will have enough energy to overcome the potential hill. They are lost from the experiment. The reflected molecules appear as a second peak at about 4.7 ms (curve n, Figure 6, inset).

This bouncing can be repeated by switching from the loading configuration back to the deceleration configuration. Because of the symmetry of the fields, the molecules undergo a reflection similar to the previous one, which results in a third peak at about 5.4 ms in curve o of Figure 6, inset. The signal intensity of the second and third peaks is almost identical because the faster molecules have already been lost. The molecules can even be reflected a third time, as seen in curve p of Figure 6, inset. Unfortunately, the molecules in lfs states are not focused in the *z*-direction and therefore will be eventually lost. This explains the decrease in intensity for the fourth peak of curve p (Figure 6, inset).

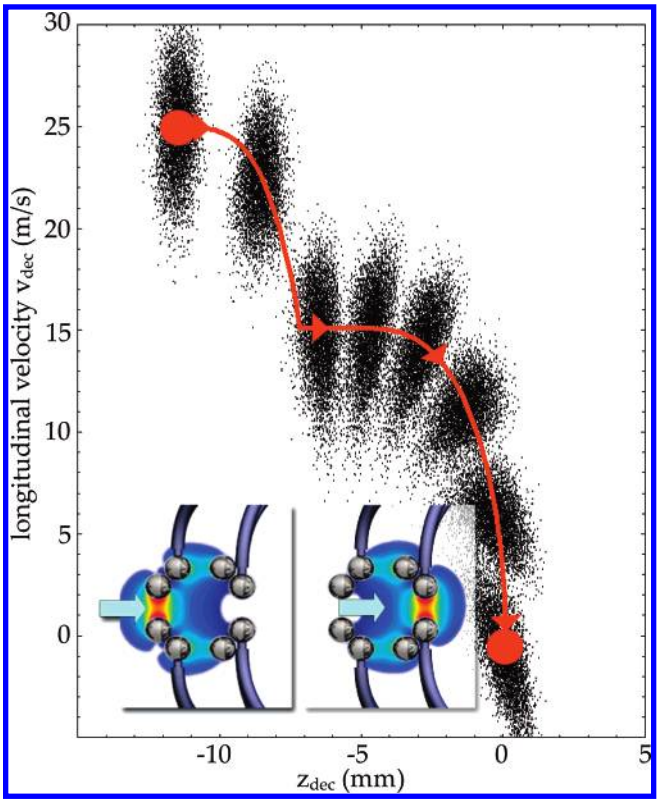

Figure 7. Snapshots in time of the phase−space distribution along the molecular beam axis for deceleration and loading. The individual snapshots are separated by equal time intervals of 100 μs. The two different processes can be nicely distinguished. The initial molecular packet leaving the decelerator and entering the trap has a mean velocity of 25 m/s and a velocity spread of ±7 m/s (FWHM). Its position is 12 mm away from the trap center, the position spread is ±1 mm (FWHM). The motion of the synchronous molecule is indicated by the orange line.

Figure 7 shows the deceleration and loading of the trap in a phase−space representation, which was obtained from our trajectory simulations. In this phase−space representation, the molecules of the decelerated packet are characterized in terms of their longitudinal velocity and their position, i.e., their distance from the trap center along the molecular beam axis. The phase−space representation is a helpful tool to understand and characterize the dynamics of the molecular packet throughout the deceleration, loading, and trapping processes. In Figure 7, the two different processes, deceleration (left-hand side) and loading (right-hand side), can be easily distinguished.

The initial packet, which left the decelerator, flies toward the trap with a mean velocity of 25 m/s and a velocity spread of ± 7 m/s (FWHM). The synchronous molecule of this packet is located 12 mm upstream from the trap center, and the position spread is typically ±1 mm (FWHM). By approaching the trap center, the molecules are decelerated. After 200 μs of deceleration, their mean velocity is reduced to 15 m/s, and their mean position is located about 7 mm upstream from the trap center. As discussed above, the focusing effect, which can be seen in Figure 6, has transverse and longitudinal contributions. Minimizing the spatial spread maximizes the velocity spread and vice versa. This results from the conservation of phase−space density, which applies to processes driven by conservative forces (Liouville's theorem). In the phase−space representation, a reduction of the longitudinal velocity spread and thus an increase

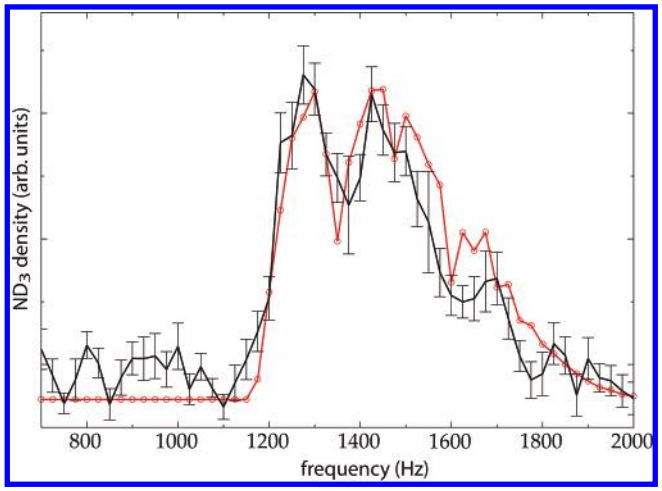

Figure 8. Frequency dependence of the density of trapped ND_3 molecules in hfs states for trapping voltages of ±10 kV after the molecules have been stored in the trap for about 60 ms. Both experimental results (with error bars) and simulations (open circles) are shown. The baseline of the Figure indicates zero signal.

in the longitudinal spatial distribution can be seen as a 90° rotation of the phase−space distribution. If the fields are turned on for longer, the distribution will rotate further. A corresponding rotation of the phase−space distribution is found for the loading. About 2 mm upstream from the trap center, the phase−space distribution is rotated by 90°. By keeping the loading fields turned on for longer, another rotation by 90° takes place. Eventually, the molecules will be brought to a standstill at the center of the trap. The velocity spread is ±5 m/s (FWHM), and the position spread is about ±1.5 mm (FWHM).

After loading the molecules into the trap, cold molecules in the hfs ground state of para-ammonia are generated using resonant microwave radiation (20 μs pulse duration). Then, the electric fields for trapping are turned on.

B. Frequency Dependence of the Trap Performance. The performance of an AC trap is highly dependent on the switching frequency. Figure 8 shows the dependence of the intensity of trapped molecules on the switching frequency for trapping voltages of ±10 kV. For all frequencies, the trap has been switched off after a complete switching cycle closest to 60 ms. As can be seen in Figure 8, experiment and simulations agree very well.

For this setup and trap voltage, the cutoff frequency is 1200 Hz, and the best trap performance is found between 1250 and 1550 Hz, whereas with increasing switching frequency (above 1700 Hz) the trap becomes shallower, and less molecules are confined. For the optimal switching frequency, we estimate that 10^4-10^5 molecules are trapped. Around 1375 Hz, a significant decrease in the number of trapped molecules is found, which is due to a nonlinear resonance with electric field terms of the fourth order.[48] Because the motion of a polar molecule confined in an AC trap corresponds to a driven oscillator,[35] it exhibits eigenfrequencies. These eigenfrequencies can be excited by the switched electric field resulting in a heating of the molecules and thus in a loss from the trap. These resonance effects are well known for ion traps but have not yet been studied in detail for dynamic traps for neutral molecules, i.e., AC traps. Around 1650 and 1800 Hz, additional resonances, which are of higher order, are found. These resonances will be investigated in more detail in a subsequent article.[48]

C. Shape of the Trapped Molecular Cloud and Trap Oscillations. In section II, we pointed out that molecules focused in the *x*-direction simultaneously experience a defocusing force

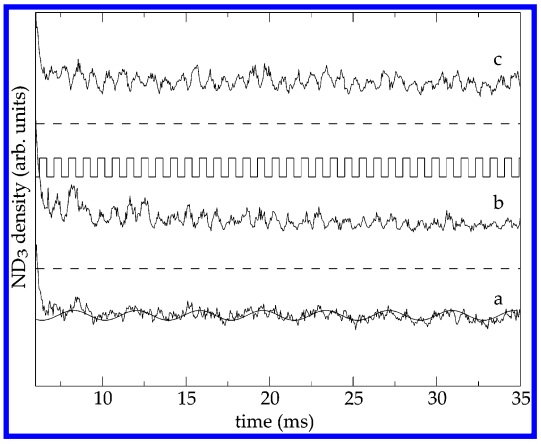

Figure 9. Evolution of the density of trapped ND_3 molecules in hfs states as a function of trapping time measured at different positions inside the trap. The dashed lines indicate the zero signal for curves b and c; the zero signal for curve a is the baseline of the Figure. For the measurements displayed in curve a, the detection laser was located 0.3 mm above the trap center, whereas for curves b and c it was 0.3 mm above the trap center and, in addition, shifted by ±0.23 mm along the molecular beam axis z_{dec}. Switching of the AC trap is indicated as well. The oscillations in curves b and c follow the switching frequency of the trap but with opposite phase. They are modulated by an additional, slower oscillation of 260 Hz (see text for details). In curve a, the amplitude of the fast oscillation is significantly reduced. The 260 Hz oscillation is more pronounced.

in the *y*-direction and vice versa. This means that the widths of the molecular packet along the *x*- and *y*-axis are oscillating between a minimum and a maximum value with the same frequency but opposite phase. This behavior also holds for the molecular density. In addition, the molecules perform an oscillation in the static electric field along the *z*-axis of the trap (Figure 3), which is calculated to have a frequency of

$$\nu = \frac{\Omega_z}{2\pi} = 265\text{Hz} \qquad (4)$$

(also see Figure 4b).

This phenomenon can be measured by placing the detection laser at different positions inside the trapping region and determining the evolution of the corresponding signal with trapping time (Figure 9). The measurements have been performed with trap voltages of ±6.6 kV and an experimentally determined optimal switching frequency of 1150 Hz. When the detection laser is placed 0.3 mm above the trapping center and +0.23 mm (curve b) and −0.23 mm (curve c) off the trapping center along the molecular beam axis z_{dec}, the detected signal oscillates with a trapping frequency of 1150 Hz but with opposite phase. The switching of the trap is indicated in Figure 9 as well. In addition, the fast oscillation is modulated by a slower one with a frequency of 260 Hz. This frequency corresponds to the oscillation of the molecules in the static electric field along the *z*-axis and is close to our calculated value of 265 Hz. In curve a of Figure 9, oscillations are shown, which were monitored 0.3 mm above the trap center but with no shift in z_{dec}. As expected, the amplitude of the 1150 Hz oscillations is significantly reduced compared to that in curves b and c, whereas that of the 265 Hz oscillations is more pronounced. When the laser is placed in the trap center, oscillations with a frequency of 510 Hz are monitored, which corresponds to twice the oscillation frequency in the *z*-direction of the trap.

D. Temperature of the Trapped Cloud and Trap Lifetime. The velocity distribution of the trapped molecules can be

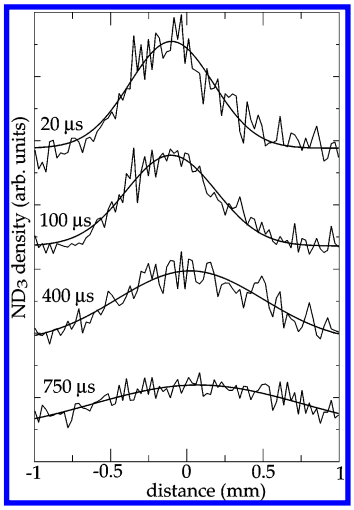

Figure 10. Spatial distributions of $^{15}ND_3$ molecules in hfs states after expansion for the time indicated in the Figure. The molecules are released from the trap after 60 switching cycles with a trapping frequency of 1150 Hz (trap voltage: ±6.6 kV). The bold lines show Gaussian fits to the distribution.

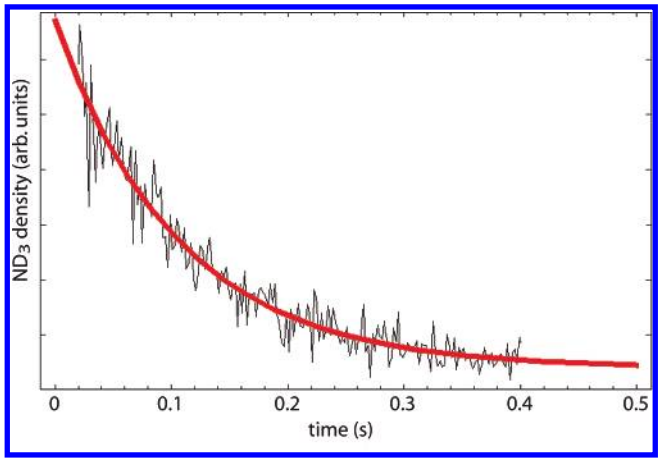

Figure 11. Density of $^{15}ND_3$ molecules in hfs states at the center of the trap as a function of trapping time. The red bold line shows an exponential fit with a $1/e = 0.11$ s lifetime. The baseline of the Figure corresponds to zero signal.

determined by measuring how rapidly the cloud expands after switching off the trap. The expansion results in less signal and an increased spatial spread. From these measurements, information about the remaining velocity spread and thus the temperature of the trapped molecules can be extracted. In Figure 10, some typical measurements of the spatial distribution of $^{15}ND_3$ molecules in the trap along the molecular beam axis are shown after letting the cloud expand for 20, 100, 400, and 750 μs. In all cases, the molecules have been trapped for about 58 ms (60 switching cycles) using a trapping frequency of 1150 Hz. The bold lines show Gaussian fits to the distribution.

From these Gaussian fits, the full spatial width at half-maximum (FWHM) of the trapped packet can be extracted for the various expansion times. If we assume that the velocity distribution is Gaussian, the cloud expands as follows

$$\Delta z_{dec}(t) = \sqrt{(\Delta z_{dec}(t=0)^2 + (\Delta v_{z,dec} t)^2)} \qquad (5)$$

with $\Delta z_{dec}(t = 0)$ being the initial spatial spread of the trapped molecules and $\Delta v_{z,dec}$ the longitudinal velocity spread along the molecular beam axis. The fitted values for the velocity spread and the initial position spread are $\Delta v_{z,dec} = 2.1$ m/s and $\Delta z_{dec}(t = 0) = 0.4$ mm, respectively. From

$$\Delta v_{z,dec} = \sqrt{(8\ln 2)}\sqrt{kT/m} \qquad (6)$$

a one-dimensional temperature (along z_{dec}) of about 2.0 mK can be deduced. The corresponding kinetic energy of the molecules is slightly lower than the simulated potential energy depth, which can be explained by imperfections of the trap geometry. As can be deduced from Figure 2, the confinement along the *x*- and the *y*-axes is stronger so that along these directions, higher temperatures, i.e., a higher kinetic energy of the molecules, can be expected. Furthermore, the deduced temperature is also dependent on the final switching phase, as has been shown in ref 35.

Figure 11 shows the evolution of the density of the trapped molecules at the center of the trap as a function of the trapping time. The red bold line through the data shows an exponential fit. Molecules are seen to escape from the trap with a $1/e = 0.11$ s lifetime. This trapping lifetime can be interpreted as being predominantly due to collisions with the background gas. The background pressure in the chamber during operation was $6 \cdot 10^{-8}$ mbar. This result is in keeping with the findings of the experiments for the cylindrically symmetric AC trap, which have been performed under similar conditions.[35] (The lifetime has been determined to be 0.17 s, and the corresponding background pressure was $4 \cdot 10^{-8}$ mbar.)

VI. Conclusions and Summary

We have experimentally demonstrated trapping of molecules in high-field seeking states using a linear AC trap. The special trapping geometry in combination with the novel way of mounting the trap offers optimal optical access as well as an improved loading scheme. Because the trap is located very close to the end of the decelerator, high intensities of the decelerated molecular packets are obtained. The loading scheme has been investigated both experimentally and theoretically in terms of a phase−space distribution. The molecules are both transversally and longitudinally focused in the course of loading, and the mean velocity is reduced to zero in the trap center. With the improved loading, loss of molecules is reduced.

The optimal switching frequency for ground-state $^{15}ND_3$-molecules has been determined to be in the range 1250−1550 Hz for trapping voltages of ±10 kV. Furthermore, resonance effects were detected. We also observed pronounced oscillations of the density of the trapped molecules as a function of trapping time, which can be explained by the spatial motion of the packet under the influence of the trapping forces. Depending on the position of our detection laser beam, we found three different oscillation frequencies: 260, 510, and 1150 Hz. The last corresponds to the driving frequency, whereas the slow oscillation (260 Hz) can be assigned to the motion of the molecular packet in the static trapping potential along the *z*-axis. All measurements have been supported by numerical simulations using the libcoldmol[41] program package.

For trap voltages of ± 6.6 kV and an optimal switching frequency of 1150 Hz, we find a full width at half-maximum (FWHM) of $\Delta z_{dec} = 0.4$ mm and $\Delta v_{z,dec} = 2.1$ m/s ($T = 2.0$ mK). From numerical simulations, we find the phase−space volume that can be confined by the trap (the acceptance) to be 50 mm^3 (m/s)^3. The phase−space volume of the Stark decelerated molecular beam (the emittance) is significantly larger than the acceptance of the trap. Therefore, we expect to spread the

molecules homogeneously over the acceptance of our trap, which is consistent with our measurements.

It is interesting to compare the linear AC trap investigated in the present work with the cylindrically symmetric trap demonstrated before[35,36] and with the three phase trap,[49] which has not been implemented yet. The acceptance of the ideal cylindrically symmetric AC trap is about 5 times larger than the acceptance of the linear AC trap. Furthermore, the cylindrically symmetric AC trap as well as the three-phase trap can be used to trap molecules in both hfs and in lfs states, which is not the case for the linear AC trap. The linear AC trap, however, is convincing with its open geometry. This not only allows optimal access for laser beams to detect and manipulate the trapped molecules but also can be crucial for sympathetic cooling experiments where a cloud of ultracold atoms, for example, has to be superimposed on the trapped molecular packet. The special double-rod design does not provide the improvements for trapping molecules in hfs states, but it allows one to maintain high electric field strengths in combination with an open-access geometry.

Acknowledgment. M.S. was supported by a Liebig stipend from the 'Fonds der Chemischen Industrie'. H.L.B. acknowledges financial support from NWO via a VENI-grant. We thank Boris Sartakov for helpful discussions.

References and Notes

(1) Doyle, J. M.; Friedrich, B.; Krems, R. V.; Masnou-Seeuws, F. *Eur. Phys. J. D* **2004**, *31*, 149.

(2) Bloch, I. *Nature Physics* **2005**, *1*, 23.

(3) Weinstein, J. D.; deCarvalho, R.; Guillet, T.; Friedrich, B.; Doyle, J. M. *Nature* **1998**, *395*, 148.

(4) Fulton, R.; Bishop, A. I.; Shneider, M. N.; Barker, P. F. *Nature Physics* **2006**, *2*, 465.

(5) Rangwala, S. A.; Junglen, T.; Rieger, T.; Pinkse, P. W. H.; Rempe, G. *Phys. Rev. A* **2003**, *67*, 043406.

(6) Rieger, T.; Junglen, T.; Rangwala, S. A.; Pinkse; P. W. H.; Rempe, G. *Phys. Rev. Lett.* **2005**, *95*, 173002.

(7) Bethlem, H. L.; Meijer, G. *Int. Rev. Phys. Chem.* **2003**, *22*, 73.

(8) Bethlem, H. L.; Berden, G.; Meijer, G. *Phys. Rev. Lett.* **1999**, *83*, 1558.

(9) Bethlem, H. L.; van Roij, A. J. A.; Jongma, R. T.; Meijer, G. *Phys. Rev. Lett.* **2002**, *88*, 133003.

(10) Bethlem, H. L.; Crompvoets, F. M. H.; Jongma, R. T.; van de Meerakker, S. Y. T.; Meijer, G. *Phys. Rev. A* **2002**, *65*, 053416.

(11) Bochinski, J. R.; Hudson, E. R.; Lewandowski, H. J.; Meijer, G.; Ye, J. *Phys. Rev. Lett.* **2003**, *91*, 243001.

(12) (a) van de Meerakker, S. Y. T.; Smeets, P. H. M.; Vanhaecke, N.; Jongma, R. T.; Meijer, G. *Phys. Rev. Lett.* **2005**, *94*, 023004. (b) Hoekstra, S.; Gilijamse, J. J.; Sartakov, B.; Vanhaecke, N.; Scarfenberg, L.; van de Meerakker, S. H. T.; Meijer, G. *Phys. Rev. Lett.* **2007**, *98*, 133001.

(13) Tarbutt, M. R.; Bethlem, H. L.; Hudson, J. J.; Ryabov, V. L.; Ryzhov, V. A.; Sauer, B. E.; Meijer, G.; Hinds, E. A. *Phys. Rev. Lett.* **2004**, *92*, 173002.

(14) Bethlem, H. L.; Tarbutt, M. R.; Küpper, J.; Carty, D.; Wohlfart, K.; Hinds, E. A.; Meijer, G. *J. Phys. B.* **2006**, *39*, R263.

(15) Hudson, E. R.; Ticknor, C.; Sawyer, B. C.; Taatjes, C. A.; Lewandowski, H. J.; Bochinski, J. R.; Bohn, J. L.; Ye, J. *Phys. Rev. A* **2006**, *73*, 063404.

(16) van de Meerakker, S. Y.; Labazan, I.; Hoekstra, S.; Küpper, J.; Meijer, G. *J. Phys. B* **2006**, *39*, S1077.

(17) Jung, S.; Tiemann, E.; Lisdat, C. *Phys. Rev. A* **2006**, *74*, 040701.

(18) Bethlem, H. L.; Berden, G.; Crompvoets, F. M. H.; Jongma, R. T.; van Roij, A. J. A.; Meijer, G. *Nature* **2000,** *406*, 491.

(19) Gilijamse, J. J.; Hoekstra, S.; van de Meerakker, S. Y. T.; Groeneboom, G. C.; Meijer, G. *Science* **2006**, *313*, 1617.

(20) Zahzam, N.; Vogt, T.; Mudrich, M.; Comparat, D.; Pillet, P. *Phys. Rev. Lett.* **2006**, *96*, 023202.

(21) Kraemer, T.; Mark, M.; Waldburger, P.; Danzl, J. G.; Chin, C.; Engeser, B.; Lange, A. D.; Pilch, K.; Jaakkola, A.; Nägerl, H. C.; Grimm, R. *Nature* **2006**, *440*, 315.

(22) Staanum, P.; Kraft, S.; Lange, J.; Wester, R.; Weidemüller, M. *Phys. Rev. Lett.* **2006**, *96*, 023201.

(23) Krems, R. V. *Phys. Rev. Lett.* **2006**, *96*, 123202.

(24) Hutson, J.; Soldan, P. *Int. Rev. Phys. Chem.* **2006,** *25*, 497.

(25) Santos, L.; Shlyapnikov, G. V.; Zoller, P.; Lewenstein, M. *Phys. Rev. Lett.* **2000**, *85*, 1791.

(26) Góral, K.; Santos, L.; Lewenstein, M. *Phys. Rev. Lett.* **2002**, *88*, 170406.

(27) Stuhler, J.; Griesmaier, A.; Koch, T.; Fattori, M.; Pfau, T.; Giovanazzi, S.; Pedri, P.; Santos, L. *Phys. Rev. Lett.* **2005**, *95*, 150406.

(28) van Veldhoven, J.; Küpper, J.; Bethlem, H. L.; Sartakov, B.; van Roij, A. J.; Meijer, G. *Eur. Phys. J. D* **2004**, *31*, 337.

(29) Hudson, E. R.; Lewandowski, H. J.; Sawyer, B. C.; Ye, J. *Phys. Rev. Lett.* **2006**, *96*, 143004.

(30) van Veldhoven, J.; Bethlem, H. L.; Schnell, M.; Meijer, G. *Phys. Rev. A* **2006**, *73*, 063408.

(31) Wing, W. H. *Phys. Rev. Lett.* **1980**, *45*, 631.

(32) Crompvoets, F. M. H.; Bethlem, H. L.; Jongma, R. T.; Meijer, G. *Nature* **2001**, *411*, 174.

(33) Shafer-Ray, N. E.; Milton, K. A.; Furneaux, B. R.; Abraham, E. R. I.; Kalbfleisch, G. R. *Phys. Rev. A* **2003**, *67*, 045401.

(34) Xu, G. Ph.D. Thesis, The University of Texas at Austin, Austin, TX, 2001.

(35) Bethlem, H. L.; van Veldhoven, J.; Schnell, M.; Meijer, G. *Phys. Rev. A* **2006**, *74*, 063403.

(36) van Veldhoven, J.; Bethlem, H. L.; Meijer, G. *Phys. Rev. Lett.* **2005**, *94*, 083001.

(37) Takekoshi, T.; Patterson, B. M.; Knize, R. J. *Phys. Rev. Lett.* **1998**, *81*, 5105.

(38) DeMille, D.; Glenn, D. R.; Petricka, J. *Eur. Phys. J. D* **2004**, *31*, 375.

(39) van Veldhoven, J.; Jongma, R. T.; Sartakov, B.; Bongers, W. A.; Meijer, G. *Phys. Rev. A* **2002**, *66*, 32501.

(40) Ashfold, M. N. R.; Dixon, R. N.; Little, N.; Stickland, R. J.; Western, C. M. *J. Chem. Phys.* **1988**, *89*, 1754.

(41) Küpper, J. *libcoldmol: A Particle Trajectory Calculation Framework*, 2003−2006. http://libcoldmol.cold-molecules.info.

(42) Townes, C. H.; Schawlow, A. L. *Microwave Spectroscopy*; Dover Publications: New York, 1975.

(43) Bhattacharjee, R. L.; Johnston, L. H.; Sudhakaran, G. R.; Sarker, J. C. *J. Mol. Spectrosc*. **1989**, *138*, 38.

(44) Heiner, C. E.; Bethlem, H. L.; Meijer, G. *Phys. Chem. Chem. Phys.* **2006**, *8*, 2666.

(45) Gubbels, K.; Meijer, G.; Friedrich, B. *Phys. Rev. A* **2006**, *73*, 063406.

(46) Schulz, S. A.; Bethlem, H. L.; van Veldhoven, J.; Küpper, J.; Conrad, H.; Meijer, G. *Phys. Rev. Lett.* **2004**, *93*, 020406.

(47) Vliegen, E.; Merkt, F. *Phys. Rev. Lett.* **2006**, *97*, 033002.

(48) Schnell, M., et al. Unpublished work, 2007.

(49) Morinaga, M.; Shimizu, F. *Laser Phys.* **1994**, *4*, 412.